THE JOURNAL OF PHYSICAL CHEMISTRY B

Article

pubs.acs.org/JPCB

Theoretical Insight into the Relationship between the Structures of Antimicrobial Peptides and Their Actions on Bacterial Membranes

Licui Chen, Xiaoxu Li, Lianghui Gao,* and Weihai Fang

Key Laboratory of Theoretical and Computational Photochemistry, Ministry of Education, College of Chemistry, Beijing Normal University, Xin-wai-da-jie 19#, Beijing 100875, China

Supporting Information

ABSTRACT: Antimicrobial peptides with diverse cationic charges, amphiphathicities, and secondary structures possess a variety of antimicrobial activities against bacteria, fungi, and other generalized targets. To illustrate the relationship between the structures of these peptide and their actions at microscopic level, we present systematic coarse-grained dissipative particle dynamics simulations of eight types of antimicrobial peptides with different secondary structures interacting with a lipid bilayer membrane. We find that the peptides use multiple mechanisms to exert their membrane-disruptive activities: A cationic charge is essential for the peptides to selectively target negatively charged bacterial membranes. This cationic charge is also responsible for promoting electroporation. A significant hydrophobic portion is necessary to disrupt the membrane through formation of a permeable pore or translocation. Alternatively, the secondary structure and the corresponding rigidity of the peptides determine the pore structure and the translocation pathway.

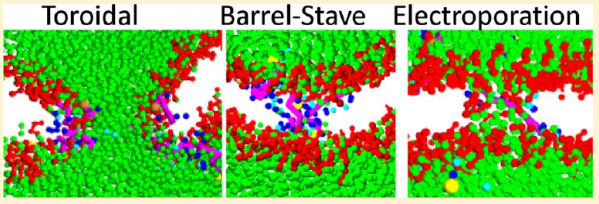

INTRODUCTION

Antimicrobial peptides (AMPs) are small and positively charged peptides produced by many tissues in invertebrate, plant, and animal species. These peptides can possess antimicrobial activities against bacteria, fungi, and other generalized targets; for example, the peptides may inhibit the replication of enveloped viruses, parasites, and even cancerous cells.[1−3] In contrast with most antibiotics, which usually target specific proteins and may have side effects, widespread resistance of AMPs has not been discovered.[4] These properties of AMPs give them an advantage as possible new therapeutic agents against the infection by pathogenic bacteria and fungi.

Currently, more than 800 different AMPs have been isolated from a wide range of organisms.[1] The diversity of the peptides makes it difficult to categorize them except on the basis of their secondary structure.[5,6] The AMPs are observed to adopt four fundamental secondary structures: α-helical, β-sheet, loop, and extended structures. Thus, the relationship between the structures and the antibiotic activities of the AMPs is interesting to study. Regardless of variations in length, amino acid composition, and secondary structure, two common features are required of the AMPs for antimicrobial activities: a cationic charge that promotes the targeting of AMPs onto the negatively charged bacterial membrane and a membrane-bound amphipathic conformation that facilitates the interaction between the AMPs and the alkyl chains.[5,6] On the basis of experimental data, it has been illustrated that the mechanism of cell death induced by AMPs may involve both membrane disruption and processes that are not membrane disruptive.[6] Membrane-disruptive peptides are thought to disrupt bacterial membranes by forming permeable holes that allow leakage of cytoplasmic components. Three models, the "barrel-stave", "carpet", and "toroidal pore" models, have been proposed to explain the membrane permeabilization.[7−9] Nondisruptive peptides are thought to act on cytoplasmic targets and to exert antimicrobial activity by inhibiting cellular processes, including DNA and protein synthesis, protein folding, enzymatic activity, and cell-wall synthesis.[6] Even for nondisruptive peptides, peptide translocation is necessary for intracellular targeting. Therefore, peptide−membrane interactions play important roles in the cell death induced by AMPs.

Limited by time and length resolution, experimental data alone are not sufficient to explain how the peptides perturb the integrity of membrane or how the peptides translocate into the cytoplasm. Alternatively, molecular simulations are useful tools in providing structure and dynamic details that cannot be easily probed experimentally.[4] Recently, molecular dynamics (MD) simulations have been used to investigate the mechanism of many peptides, such as Magainin,[10] Melittin,[11] HIV-1 Tat,[12] and cyclic peptides[13] interacting with model phospholipid membranes. Pore formation and micellar disaggregation mechanisms have been suggested by simulations. However, the all-atom simulation is still limited to systems containing a few hundred lipids and a couple of peptides on a nanosecond time scale. In contrast, the peptide-induced cell death covers time scales from nanoseconds to seconds and involves thousands of lipids. Coarse-grained (CG) models are required

Special Issue: William L. Jorgensen Festschrift

Received: June 3, 2014
Revised: July 22, 2014

dx.doi.org/10.1021/jp505497k | J. Phys. Chem. B XXXX, XXX, XXX−XXX

to simulate these processes on larger systems and longer time scales without losing realistic structure details.

In CG modeling, a few atoms are grouped into one quasiparticle (or bead) by averaging out some set of nonessential degrees of freedom.[14,15] Thus, coarse graining allows MD to simulate systems with sizes up to the micrometer range and on time scales approaching milliseconds.[15] Several CG approaches have been used to study peptide−membrane systems, such as the implicit solvent CGMD method,[16] the explicit solvent CGMD method,[17] and the dissipative particle dynamics (DPD) method with explicit solvent.[18−20] Among these approaches, the DPD method has been actively applied to model self-assembled systems because it explicitly includes the random and dissipative forces produced by the reduction of the degrees of freedom.[21−24] This method can bridge the atomic scale and the hydrodynamic scale. In our previous work, we employed DPD to simulate the action of peripheral and transmembrane peptides on the membrane.[18−20] In that work, very simplistic rigid rod peptide models were used. The detailed secondary structure and amphipathicity were not considered. In this study, we construct more refined α-helical (Magainin 2, MG-H2, Melittin, CM15), β-sheet (Protegrin-1, Tachyplesin I), and extended (HIV-1 Tat, Indolicidin) DPD peptide models to illustrate their diverse actions on the model membrane. To reproduce realistic geometric and thermodynamic properties of the bilayer membrane and peptides, based on the functional group, we divided the CG beads into types distinguished by polarizability and hydrogen-bonding capacity.[25,26] Optimized DPD force parameters transferrable for both lipids and amino acids and developed recently by us are applied to the interacting systems of AMPs and membrane. Our simulations illustrate well the relationship between the peptide activities and their charge distribution, amphipathicity, and secondary structure at the molecular level: First, the cationic charges of the peptides are essential to selectivity for the negatively charged microbial membrane. The peptides also attract anionic lipids and increase the local membrane potential, which may, in turn, cause electroporation. Second, well-defined amphipathic portions are essential for peptides to penetrate into the membrane and disrupt the order of the lipid around them. The disruption induces membrane compression (or tension) and corrugation in the incubation phase, and these effects cause permeable pores or peptide translocation in the active killing phase. Lastly, the secondary structure of the peptide determines the pore structure and the translocation pathway. AMPs with α-helical structures are the most rigid and favor forming stable and permeable pores inside the membrane. β-sheet AMPs are relatively flexible, tend to form stable pores, and can also translocate across membrane through the pores. Extended AMPs are more flexible; this flexibility facilitates translocation across membrane via short-lived pores. These multiple modes of action work together to maximize the efficiency of the peptide activity.

COARSE-GRAINED MODEL AND METHOD

In the CG DPD simulation, the elementary units are soft beads with mass m and diameter r_0.[21,22,27] Each bead represents a fluid volume of several molecules. Here we use a four-to-one mapping scheme to construct the CG model.[17,25,26] Water is explicitly modeled as a single bead (denoted by W), which represents four water molecules. Accordingly, the physical bead size r_0 is set to 0.71 nm.[22,27] A lipid molecule is modeled as a polymer consisting of hydrophilic and hydrophobic beads. An amino acid residue is represented by one backbone bead and one or more side-chain beads. The atomic representations of a DMPC (dimyristoylphosphatidylcholine) lipid and five examples of protein amino acids and their corresponding CG models are given in Figure 1. Similar to the MARTINI model,[17,25,26]

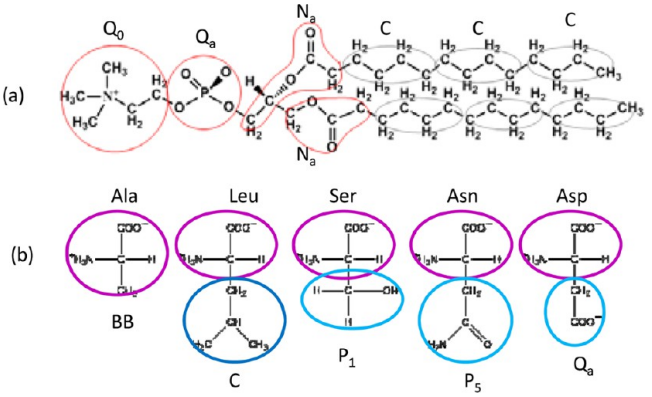

Figure 1. Coarse-grained mapping of DMPC lipid and sampled amino acids.

the DPD beads are sorted into charged (Q), polar (P), nonpolar (N), and apolar (C) types. Each type is further divided into sublevels with hydrogen donor capacities (d), hydrogen acceptor capacities (a), and lack of hydrogen bond forming capacities (0). Accordingly, as shown in Figure 1, the choline group of the DMPC head is type Q_0, the phosphate group of is type Q_a, the poly(ethylene oxide) group is type N_a, and the hydrocarbon group is type C. The bilayer membrane chosen here also comprises DMPG (dimyristoylphosphatidylglycerol) lipid. The glycerol group containing hydroxyl groups is assigned type P1. For the side chains of the amino acids, the amide group is type P_5 with strong polarity, the hydroxyl group or hydrosulfide group is type P_1 with intermediate polarity, and the hydrocarbon group is type C. The type of the backbone beads (BB) of the amino acids depends on the secondary structure of the polypeptide:[17] In a coiled or bent structure, the bead is a strongly polar P_5 type. In an α-helical or β structure, the polarity is reduced because of the hydrogen bonding between the backbones. Therefore, the bead is the nonpolar N_0-type for an α-helical structure and the N_{da}-type for a β-structure.

In the DPD simulations,[21,22] all of the beads interact through a short-ranged repulsive conservative force

$$F_{ij}^{C}(r_{ij}) = a_{ij}(1 - r_{ij}/r_0)\hat{\mathbf{r}}_{ij} \quad (1)$$

a random force

$$F_{ij}^{R}(r_{ij}) = \sqrt{2\gamma_{ij}k_BT}(1 - r_{ij}/r_0)\zeta_{ij}\hat{\mathbf{r}}_{ij} \quad (2)$$

and a dissipative force

$$F_{ij}^{D}(r_{ij}) = -\gamma_{ij}(1 - r_{ij}/r_0)^2(\hat{\mathbf{r}}_{ij}\cdot\mathbf{v}_{ij})\hat{\mathbf{r}}_{ij} \quad (3)$$

for two beads with a separation $r_{ij} < r_0$.[22] Here each vector $\mathbf{v}_{ij} \equiv \mathbf{v}_i - \mathbf{v}_j$ is the velocity difference between particles i and j. The parameters a_{ij} (in units of k_BT/r_0) represent the repulsion strengths. The friction coefficients are γ_{ij} [in units of $(k_BTm_0/r_0^2)^{1/2}$]. The ζ_{ij} are symmetrically and uniformly distributed random numbers. Fine-tuned force parameters a_{ij} for the phospholipid and amino acid models are listed in Table 1. The

dx.doi.org/10.1021/jp505497k | J. Phys. Chem. B XXXX, XXX, XXX−XXX

Table 1. DPD Force Parameter a_{ij}

aij (k_BT/r_0)	W	Q_0	Q_d	Q_a	N_a	C	P_S	P_1	N_0	N_{da}
W	78	72	72	72	79.3	104	72	79.3	86.7	79.3
Q_0		86.7	79.3	79.3	79.3	104	78	79.3	86.7	79.3
Q_d			86.7	72	78	104	72	78	86.7	78
Q_a				86.7	79.3	104	72	78	86.7	78
N_a					79.3	94	78	79.3	86.7	79.3
C						78	104	104	94	94
P_S							72	72	86.7	78
P_1								79.3	79.3	78
N_0									86.7	86.7
N_{da}										78

γ_{ij} have values 4.5, 9, and 20 corresponding to low, intermediate, and high values of a_{ij}.[22,27]

All of the bonds interacts through harmonic potential[23,24]

$$E_2(r) = \frac{1}{2}K_2(r - L_0)^2 \quad (4)$$

The spring constant K_2 for all bonds is set to be 128 (in units of $(k_BT/r_0^2)^{1/2}$). The spring length L_0 is $0.6r_0$ for the tails of the DMPC molecule and $0.5r_0$ for the lipid headgroup and peptides. The stiffness of bond bending is described by

$$E_3(r) = K_3[1 - \cos(\theta - \theta_0)] \quad (5)$$

For DMPC, the values of K_3 are all set to 10 k_BT, and the angles are 180° with the exception of $\angle Q_a - N_a - N_a$, which is 120°.

A dissociable Morse potential is introduced between the beads of the skeleton to mimic the hydrogen bonding that stabilizes the α-helical and β-sheet structures of peptides[28]

$$E_M(r) = K_M[1 - e^{-\alpha(r-r_e)}]^2 \quad (6)$$

For a helical structure, one to three Morse bonds are introduced between two backbone beads separated by two harmonic bonds, and one to five Morse bonds are introduced between beads separated by four harmonic bonds. Here the equilibrium distance r_e is set to $0.5r_0$ for the one to three Morse bonds and $0.75r_0$ for the one to five Morse bonds. The width of the potential well is set to $\alpha = 6.4r_0$. The cutoff is set to $r_M = 2.0r_0$. The depths of the potential well K_M are 3 and 6 k_BT for the one to three Morse bonds and the one to five Morse bonds, respectively. Two backbone beads with hydrogen bonds are connected by one to three Morse bonds to restrain the β structure. In β strands, a one-to-three harmonic bond potential is applied to two backbone beads separated by two bonds.

The electrostatic interactions between charged beads are calculated using the method introduced by Groot.[29] Here the charges are distributed on a lattice and the electrostatic field is solved locally on the grid. The force and the virial contributed by the self-energy term are subtracted from the total force of each charged bead and the total virial as discussed in detail in our recent paper.[30] The values of the electrostatic parameters used are the same as in ref 30. Because DMPC is a zwitterionic lipid, we found that explicitly considering the electrostatic interactions of the DMPC head groups has a negligible effect on the membrane properties. For example, the area per lipid for the tensionless pure DMPC bilayer is 0.69 nm^2 when simulation is performed without explicitly considering the electrostatic interactions of the head groups. When they are considered explicitly, the area per lipid increases to 0.70 nm^2. The membrane thickness for these two cases is 3.66 and 3.69 nm, respectively. Thus, in this work, the electrostatic interactions of the DMPC head groups are not explicitly calculated to save simulation time. However, the charges on the DMPG, the peptide, and their counterions are explicitly considered.

The structure and thermodynamic properties of the DMPC are well-reproduced by this parameter set. In addition, the lipid bilayer obtained by this force field can only resist <10% strain before rupture, and this behavior closely resembles a real lipid membrane.

To prepare a lipid bilayer, 1600 lipid molecules composed of 80% DMPC and 20% DMPG are placed in the center of a $33.5r_0 \times 33.5r_0 \times 32r_0$ sized box with the head groups in the outside and the alkyl chains inside the membrane. The addition of DMPG lipid with its negatively charged headgroup is to mimic the bacterial membrane; the headgroup enhances the affinity of the peptides for the membrane. The anionic DMPG counterions and the water beads are distributed randomly in the space unoccupied by the membrane. The entire system has a bead density of $\rho = 3$. These simulations are first performed in the constant surface tension and constant temperature ($N\gamma_sP_\perp T$) ensemble[30,31] for 50 000 time steps to achieve bilayers without tension. Here the time step is set to $0.02t_0$, which corresponds to 2.86 ps.[27] Then, 8, 16, or 32 peptides and their counterions are added to the simulation box by removing the same number of water beads to maintain a density of $\rho = 3$. The initial CG structures of the AMPs Magainin 2, MG-H2, Melittin, CM15, Protegrin-1, Tachyplesin I, HIV-1 Tat, and Indolicidin are all obtained from the Protein Data Bank, as shown in Figure 2. These peptides are placed 2 nm above the upper leaflet of the bilayer membrane. Then, each simulation is run for up to 800 000 time steps (~1.136 μs) in the NVT ensemble. For each system, five parallel samples are simulated to collect data. All of the simulations are performed under periodic boundary condition. The NVT ensemble is chosen to mimic the peptide−vesicle systems, where the vesicle has volume confinement. It is also easy to test whether the membrane undulation induced by the peptide adsorption is Euler buckling under NVT boundary conditions.[20] In our previous work, we simulated the interactions between peptide and bilayer membrane in both $N\gamma_sP_\perp T$[18−20] and NVT ensembles.[20] Similar behaviors, such as membrane buckling, peptide translocation, and membrane pore formation, were all observed in both ensembles. It indicates that the effects of AMPs on the membrane integrity are independent of the ensembles.

dx.doi.org/10.1021/jp505497k | J. Phys. Chem. B XXXX, XXX, XXX−XXX

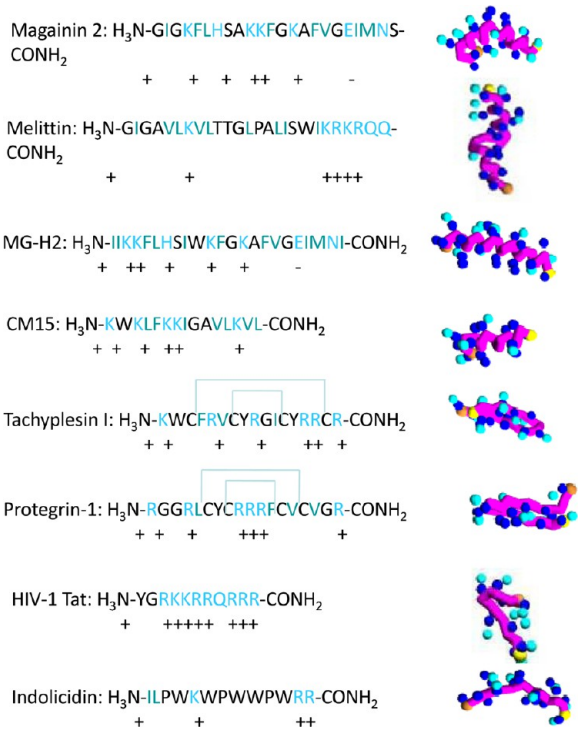

Figure 2. Residue sequences and coarse-grained structures of eight antimicrobial peptides. The backbone of the peptide is represented by magenta bonds. The hydrophilic side-chain bead is cyan, and the hydrophobic side-chain bead is blue. The N and C termini are colored in gold and yellow for distinction.

RESULTS

***α*-Helical AMPs Induce Stable Pores in the Bilayer Membrane.** Magainin 2, MG-H2 (an analogue of Magainin), Melittin, and CM15 fold into *α*-helices when they bind to bilayer membrane with well-separated amphiphathic regions.[32−34] The sizes of the hydrophilic and hydrophobic regions are comparable for both Magainin 2 and Melittin.[35] Magainin 2 has a slight bend in the center at residue 12 and 13, whereas the helical conformation of Melittin is interrupted at residues 10 to 12. In Magainin 2, the charge is distributed along the helical axis, but in Melittin, the charge is primarily located near the C-terminus. CM15 is a synthetic hybrid AMP composed of the first seven residues of cecropin A and residues 2−9 of Melittin.[34] CM15 has a highly cationic N-terminal region and a hydrophobic C-terminal region. The similarity in the *α*-structure and the differences in the charge distribution and amphilicity of these AMPs may result in similar peptide activities with minor differences.

We first simulate the interactions between Magainin 2 and a bilayer membrane. When there are only eight Magainins with peptide/lipid (P/L) molar ratio of 0.5/100, the peptides are adsorbed onto the membrane with their helical axes oriented parallel to the surface of the membrane. Their hydrophilic faces extend into the solvent, whereas the hydrophobic faces are buried into the hydrocarbon core of the membrane. The binding of Magainin 2 to the membrane compresses the lipids on the proximate leaflet and induces membrane buckling, as shown in Figure 3a. However, at such a low peptide concentration, the integrity of the membrane is not disrupted. Only one peptide translocates across the bilayer via a transient small pore, shown in Figure 3b. Such a pore usually occurs by

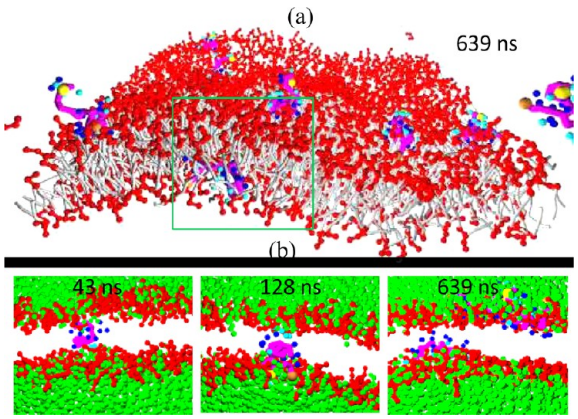

Figure 3. Snapshots of eight Magainin 2 peptides interacting with a bilayer membrane. (a) Overview of the peptide−membrane complex. (b) Time sequence of the cross-sectional view of the complex and focuses on the translocation of one Magainin as squared in panel a. For clarity, the hydrophobic tails of the lipids are invisible.

fluctuations in regions with high local peptide concentrations. The lifetime of this pore is <400 ns.

When the P/L molar ratio increases to 1/100, the adsorption of Magainin 2 onto the bilayer induces even stronger membrane buckling, as shown in Figure 4. Following the membrane corrugation, one or two AMPs insert into the membrane and form a small pore. Later on, more peptides and lipid head groups are able to enter the pore and enlarge it to an intermediate-sized stable and permeable pore. Here each pore comprises two to three peptides. The interior diameter of the pore is estimated to be ∼1.8 to 3.6 nm. Water can transport across the pores. Near the mouth of the pore on the upper leaflet, one or more peptides are also observed and are only partially inserted into the pore. This pore resembles the disordered toroidal model[32] and is consistent with the all-atom MD results.[10] Far from the pores, the AMPs remain in parallel to the membrane surface. Few or even no peptides are found to translocate across the membrane via the pores.

At even higher peptide concentrations, for example, at P/L = 2/100 and 4/100, much larger permeable pores can form; see Figure 5a. Up to five to six peptides are found inside the pore. Some of these huge pores are formed through fusion of two intermediate sized pores. Unlike the intermediate-sized pore, which resembles a cylindrical hole, the huge pore is irregularly shaped. Actually, the membrane is even broken into a micelle-like structure as P/L ratio approaches 4/100; see Figure 6. This type of disruptive action of Magainin 2 on the membrane is more similar to the carpet model.[7−9] This observation supports the view that the carpet model is an extreme extension of the toroidal pore model at high peptide concentrations.[2]

We also simulated an analogue of Magainin 2, the so-called MG-H2 peptide. (The residues are given in Figure 2.) MG-H2 has relatively higher hydrophobicity compared with its parent.[36] This peptide can induce the formation of multipermeable pore at concentrations as low as p/L = 0.5/100. However, the pore size does not change much as additional peptide binds the membrane. Even when P/L molar ratios approach 2/100 and 4/100, each pore contains only one or two peptides, as shown in Figure 5b.

We then simulated Melittin−membrane systems at P/L molar ratios of 0.5/100, 1/100, 2/100, and 4/100. Similar to Magainin 2, Melittins begin to disrupt the membrane integrity

dx.doi.org/10.1021/jp505497k | J. Phys. Chem. B XXXX, XXX, XXX−XXX

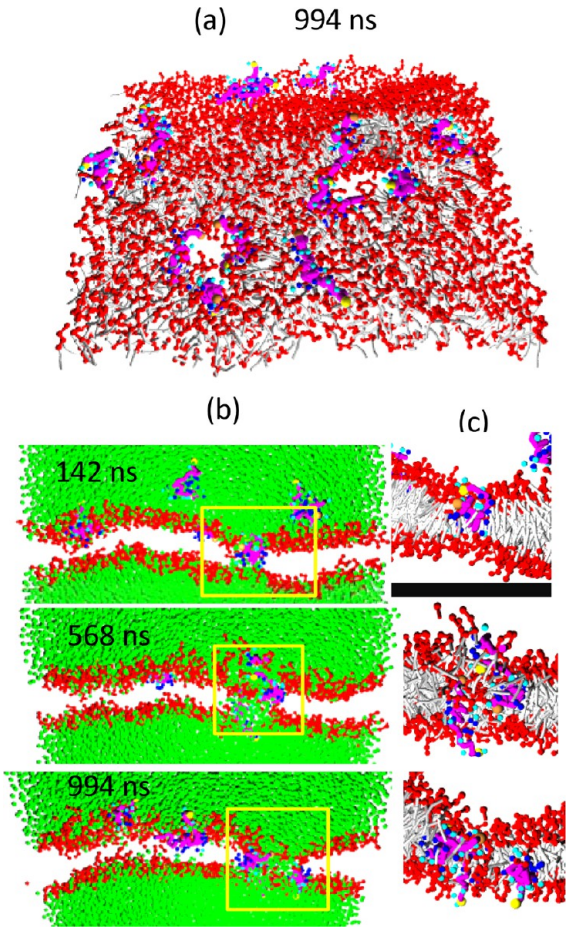

Figure 4. Snapshots of 16 Magainin 2 peptides interacting with a bilayer membrane. (a) Overview of the peptide−membrane complex. To see the pore structure, we cut the membrane into four slices. (b) Time sequence of the cross-sectional view of one of the slices. (c) Pore structure as squared in panel b.

when the P/L molar ratio approaches or exceeds 1/100. Melittin also induces membrane buckling and forms disordered toroidal pores in the membrane. The pores induced by Melittin is smaller than that induced by Magainin 2 but bigger than that induced by MG-H2. A few AMPs can translocate across the membrane via the pore, as shown in Figure 5c. In experiments on giant vesicles, Melittin translocation and redistribution was found on both sides of the membrane.[33] At P/L = 4/100, membrane lysis induced by Melittin resembles micellar disaggregation, as shown in Figure 6.

In contrast with Magainin and Melittin, CM15 disrupts the bilayer membrane by perpendicularly inserting into the membrane and forming nonpermeable worm-hole-like pores. Here each hole is composed of only one peptide and few or no lipid head groups, as shown in Figure 5d. This is in agreement with experimental results showing that CM15 does not form stable aggregates.[34] The specific structure of CM15 with its cationic charge-rich N-terminal region and hydrophobic C-terminal region makes it behave like a giant amphiphilic lipid molecule. CM15 favors insertion into the bilayer with its hydrophilic N-terminal region extending into the lipid head−solvent interface and its hydrophobic C-terminal region penetrating deeply into the membrane core. The insertion ability of CM15 is almost independent of the peptide concentration. At P/L molar ratios as low as 0.5/100, all of the peptide can enter into the membrane and induce membrane curvature. Detailed evolutionary structure of the peptide insertion state is given in Figure 7. We can see that when the peptides start to insert into membrane, they attach to a few water beads and lipid head groups. But the water and lipid heads stay in the pores for only <100 ns. They move along the inserted peptides and finally reach to the ultimate leaflet of the bilayer. It indicates that the peptide translocation is rare, but the flip-flops of the lipid are promoted during the process of peptide insertion. We find that for the peptide−membrane systems containing 8, 16, and 32 CM15, approximately 5, 15, and 20 lipids are correspondingly observed flip-flopped in 1.14 μs. For the pure lipid bilayer system, only two or three lipids can flip-flop on the same time scale.

β-Sheet AMPs Translocate Across the Membrane via Stable Pores. The β-sheet conformations of Protegrin-1[37,38] and Tachyplesin I[7,39] are stabilized by disulfide bridges between the conserved Cys residues. Thus, the β-sheet structure of this type of peptide does not exhibit any differences in lipid and aqueous environments. However, these peptides still have amphipathicity. The major difference between these two AMPs is that for Protegrin the anionic charged residues are clustered in the turn region and in the tails; for Tachyplesin, the charges extend along the two strands, but one chain has polar side chains and the other contains apolar side chains. These peptides exert activities similar to Magainin 2 and Melittin.

At P/L molar ratios less than 1/100, both the Protegrin and Tachyplesin monomers bind onto the membrane surface in the parallel orientation. Because each Protegrin-1 or Tachyplesin peptide contains seven canionic charges, the strong electrostatic repulsions inhibit the formation of dimers or oligomers. When the P/L molar ratio increases to 1/100 or more, permeable pores start to form, as shown in Figure 8. The Protegrin-1-induced pores are more stable and larger. Usually, each pore comprises two to four peptides and resembles the toroidal model.[7−9] This feature may be caused by the charge clustering in the turn and tail regions. The two hydrophilic caps make Protegrin favor the transmembrane state. In contrast, the Tachyplesin-induced pores are smaller and more disordered. The peptides are primarily located near the mouth of the pore on the two leaflets. Similar to Melittin, Protegrin-1 and Tachyplesin I peptides can translocate across the membrane via the pores, and these results are also consistent with experiments.[7,37−39] The frequent peptide translocation reduces the possibility of micellar disaggregation. Even when the P/L ratio is as high as 4/100, these two β-sheet AMPs cannot break off the membrane.

Extended AMPs Translocate Across the Membrane via Short-Lived Pores. The Indolicidin[40,41] and HIV-1 Tat (residues 37−47 of HIV-1 Tat protein) peptides[42] containing high proportions of Arg and Trp residues do not fold into regular secondary structures and are in extended conformations. We find that these highly charged small peptides also exhibit antimicrobial activities by inducing pores and translocation across the membrane.

Indolicidin adsorbs onto the membrane surface and inserts into the membrane in a manner similar to that of the β-sheet AMPs; see Figure 9. Indolicidin can trigger multipores at concentrations as low as P/L = 0.5/100. Because of its smaller size and flexibility, Indolicidin induces pores that are irregular and small and only contains 1−3 peptides. In the early stages, the newly created pore may include peptides, lipid head groups and water, or only peptides. However, the permeable pore is

dx.doi.org/10.1021/jp505497k | J. Phys. Chem. B XXXX, XXX, XXX−XXX

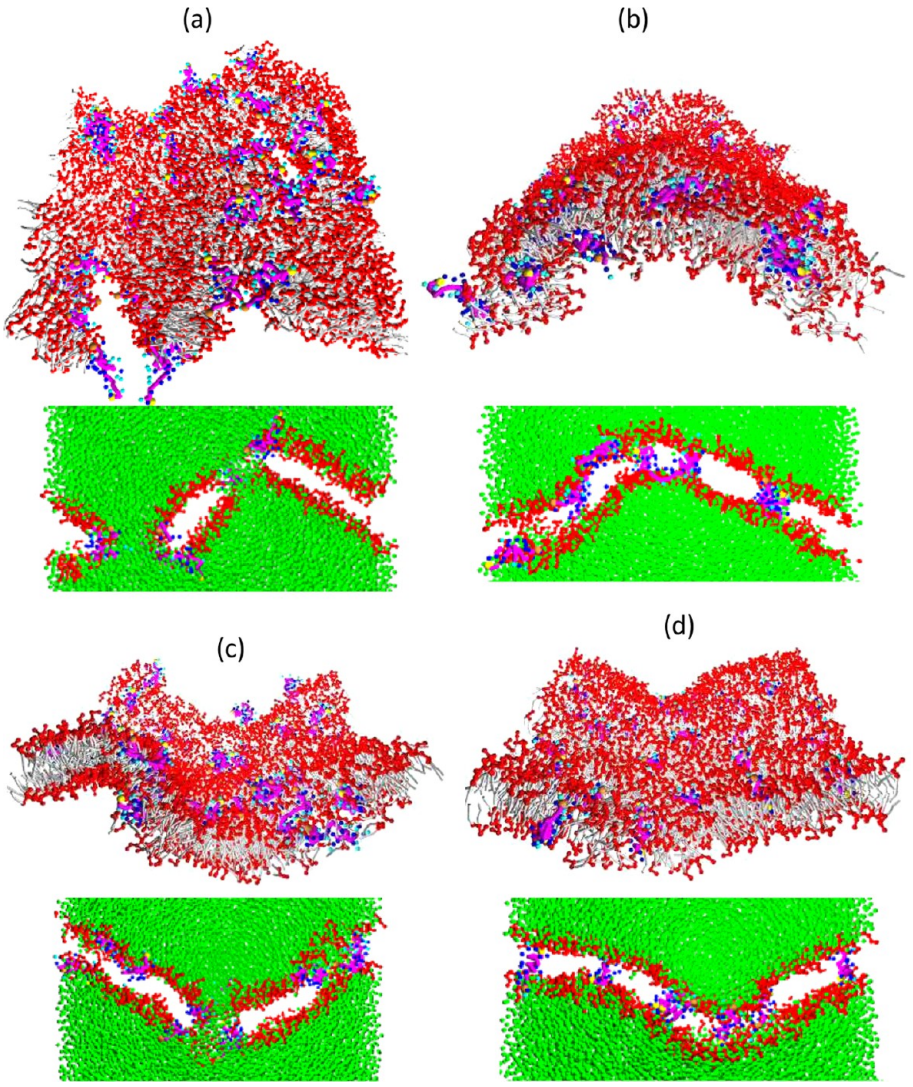

Figure 5. Snapshots of 32 (a) Magainin 2, (b) MG-H2, (c) Melittin, and (d) CM15 peptides interacting with a bilayer membrane at a simulation time of 1.136 μs.

transient. Water and lipids move quickly downward or even upward back to the membrane surface so that only a few peptides remain inside the pore. This pore is similar to the irregular barrel-stave model. Indolicidin itself also has the potential to translocate across the membrane via the pores. Following this movement, another peptide previously located near the mouth of the pore on the upper leaflet may also enter the pore. During this process, the pore does not open much. Some experiments indicated that Indolicidin can induce discrete channels[41] but does not lyse bacterial cells.[40] These experiments support our observations.

The HIV-1 Tat peptide has very weak hydrophobicity, so it does not penetrate deeply into the membrane surface upon binding. In fact, the peptides float on the membrane−solvent interface without causing significant membrane curvature, as shown in Figure 10a. Nevertheless, this peptide still has the ability to form water pores in the bilayer when enough peptides are affiliated with the membrane. However, in contrast with the pores induced by all of the other AMPs studied in this work, the surface of the HIV-Tat peptide-induced pore is purely composed of lipid head groups. A few peptides can flux through the water pore one by one. Then, the pore reseals when no additional peptides follow. Figure 10b and the movie in the Supporting Information illustrate this translocation process well. This observation is consistent with both experiments[42] and all-atom MD simulations,[12] showing that HIV-1 Tat peptides can translocate through the plasma membrane via transient pores and accumulate in the cell nucleus.

DISCUSSION

Experiments can probe the functions of AMP on a macroscopic level but lack the detailed information on the structure of the membrane-peptide complex and the dynamics of the cell-death process. All-atom MD simulations can provide molecular structures of the membrane-peptide complex in a short-time window but are still unable to describe the "long" action process of the peptide-induced cell death. Alternatively, our coarse-grained DPD simulations well bridge the microscopic and macroscopic levels. Our results show that various AMPs exert their activities on the membrane by inducing pores with different structure or by translocating across the membrane through different pathways, as listed statistically in Table 2. The broad spectrum activities are related to the charges, amphipathicity, and secondary structure of the AMPs. In the

dx.doi.org/10.1021/jp505497k | J. Phys. Chem. B XXXX, XXX, XXX−XXX

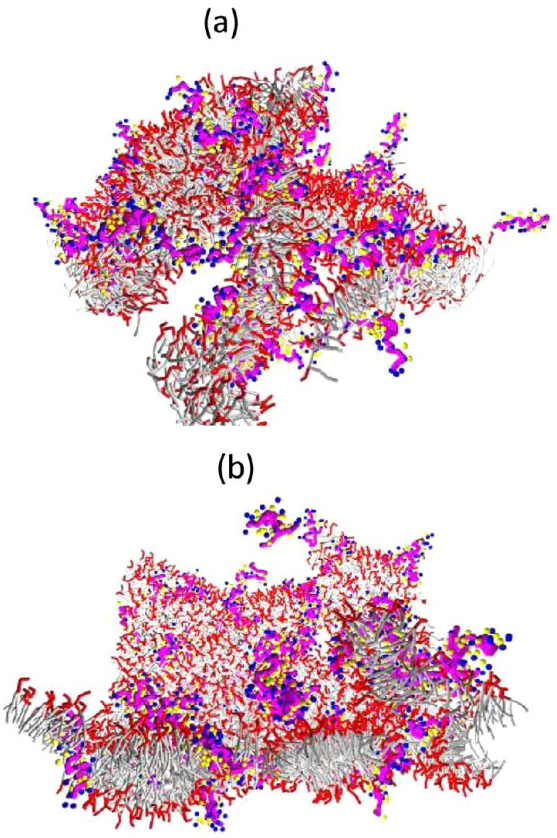

Figure 6. Snapshots of 64 (a) Magainin 2 and (b) Melittin peptides interacting with a bilayer membrane at a simulation time of 1.136 μs.

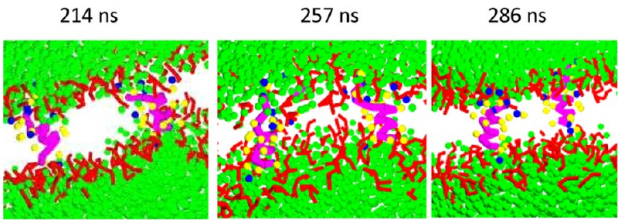

Figure 7. Evolution of two pores induced by 32 CM15 peptides interacting with a bilayer membrane.

following subsections, we will discuss the active mechanisms in detail.

Cationicity. Cationic charge is a common feature for AMPs; it promotes selectivity for the negatively charged microbial membrane. All of the peptides we chose in this study can bind to the membrane containing 20% anionic DMPG lipid through electrostatic attraction. A counter-example is Alamethicin, which carries no charge. We find (data not shown) that this peptide does not bind to the membrane except by being placed very close to the surface of the membrane. In addition to facilitating targeting, our simulation reveals that the charge also plays important roles in membrane poration, as for the HIV-1 Tat peptide. This peptide has few hydrophobic residues, so it binds only to the water−lipid-head interface without penetrating deeply into the hydrophobic core of the membrane. From this perspective, this peptides does not seem to be able to disrupt the membrane and exert killing activity. However, the peptide can still cause the formation of transient pore permeable to water and itself. In contrast with the disordered toroidal pore or barrel-stave pore in which the surface of the pore is peptide-and-lipid-lined, the HIV-1 Tat peptide-induced pore is lined only with lipid head groups. Peptide efflux resembles electroporation model.[43] This finding suggests that the highly charged cationic peptides promote the accumulation of anionic lipids on the upper leaflet and increase the membrane potential. Above a threshold potential, electroporation occurs.[43] To verify such effects, we calculate the normal component of the averaged electric field as a function of distance Z from the middle of the membrane,[29,30,43,44] as given in Figure 11. It is obtained from the average of time over 20 ns just before pore formation. We find that the electric fields across the membrane induced by HIV-1 Tat peptides are 0.36 and 0.46 V/nm for systems containing 8 and 16 peptides, respectively. They are close to the critical value of 0.4 V/nm to induce pore formation by external electric field.[44,45] For comparison, we also calculate the normal electric-field distribution for the pure DMPC/DMPG bilayer membrane and Magainin 2-membrane complexes. There is roughly a zero electric field in the hydrophobic interior of the pure bilayer without peptide bound. Compared with HIV-1 Tat peptide, Magainin 2 peptide carries only half charges. As a result, we find that the electric field across the membrane caused by the binding of Magainin 2 peptides is <0.2 V/nm even at P/L = 1/100, where permeable pores can form. Such membrane potential is not enough to induce pore formation by itself. Therefore, for Magainin 2 and other peptides with relatively less cationic charges, the electroporation mode perhaps combines "dirtily" with other modes,[5] such as amphipathicity, to disrupt the integrity of the membrane, as will be discussed in the following subsections.

Amphipathicity. Amphipathicity is essential for AMPs to disrupt the order of the membrane. The peptides selected here (except for HIV-1 Tat peptide) all have significant hydrophobic portions. Upon binding to the membrane, the hydrophobic portions penetrate into the hydrophobic core of the bilayer and occupy the space beneath the membrane surface. Such binding induces asymmetric compression and tension on the two leaflets and causes strong membrane corrugation (or buckling) when sufficient peptides adsorb onto the bilayer. For many peptides, usually the hydrophobic lengths of AMPs and lipids do not match, and the mismatch results in membrane thinning. The membrane corrugation and thinning occur during an incubation phase in which the membrane integrity is still maintained.[46] However, when the local asymmetrical tension of the membrane exceeds the critical value of rupture, the peptides will associate with lipids to insert into the membrane and form pores. The corrugated incubation phase transits to the execution phase.

Comparing Magainin 2 with MG-H2, we can see that the amphiphilicity of the peptides can also affect the number and size of the pores. Peptides with larger hydrophobic portions can penetrate deeply into the membrane and can strongly disrupt the order of the lipids around them. To see these effects, we calculate the averaged orientation order of the lipid tails around Magainin 2 and MG-H2 peptides, $S = 0.5(3\cos\theta - 1)$. Here θ is the angle between the direction of the lipid tail and the normal direction of the membrane. The calculations are performed for systems containing eight peptides. The data are the average of time over 30 ns; in that time interval, the peptides are fully adsorbed to the membrane surface but do not insert into the membrane yet. Only lipids in distance (on X−Y plan) <3 nm from the peptide are considered. We find that Magainin 2 peptides reduce the lipid tail order from 0.55 (bulk

dx.doi.org/10.1021/jp505497k | J. Phys. Chem. B XXXX, XXX, XXX−XXX

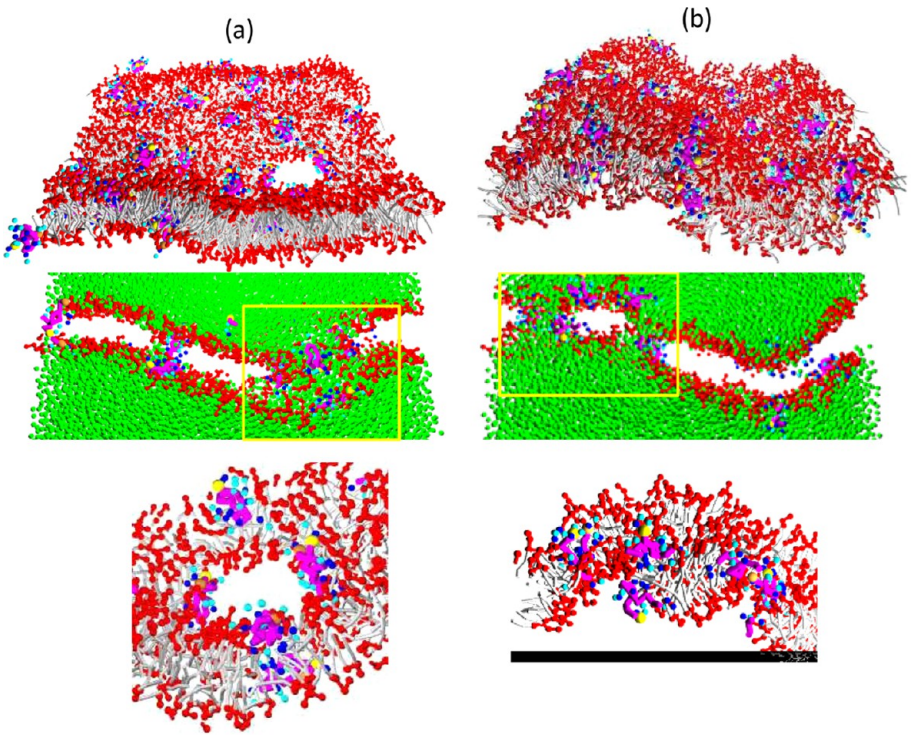

Figure 8. Snapshots of 32 (a) Protegrin-1 and (b) Tachyplesin I peptides interacting with a bilayer membrane at a simulation time of 1.136 μs.

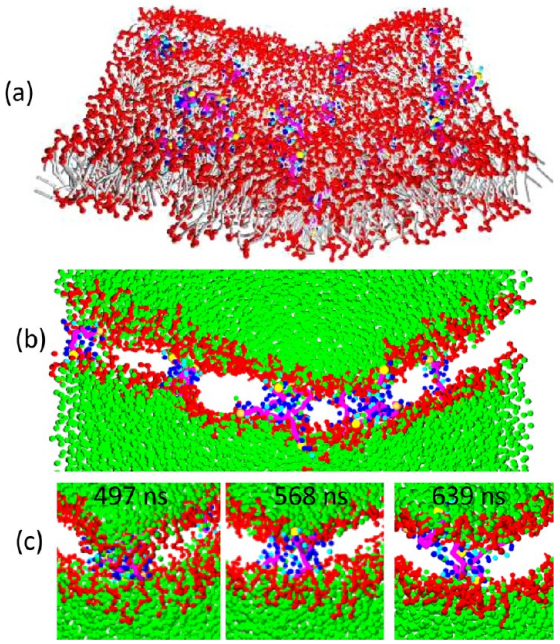

Figure 9. Snapshots of (a) the overview and (b) the cross-sectional view of the peptide−membrane complex containing 32 Indolicidin AMPs at 1.136 μs. (c) Evolution of an irregular barrel-stave pore.

value) to 0.53 (around the peptides), while MG-H2 peptides with larger hydrophobic portions reduce it to 0.50. Thus, at relatively low peptide concentrations, a few of the peptides with large hydrophobic portions can induce high membrane curvature and promote small multipores. In contrast, more peptides with larger hydrophilic portions are needed to form a pore. Once a pore is created, its size increases quickly because the large hydrophilic face of the peptide tends to associate with more water and lipid heads. Similarly, the charges accumulating in the terminal regions of Melittin make its penetration relatively shallow. Therefore, compared with Magainin 2, the size of the pore induced by Melittin is relatively smaller.

The amphipathic structure of CM15 is different from that of other α-helical peptides. CM15 is like a lipid molecule with a hydrophilic head and a long hydrophobic tail. The insertion of CM15 into the bilayer only induces membrane corrugation but does not induce significant membrane thinning. In agreement with experiment,[34] the changes in dynamics of lipid motion are minimal and occur primarily near the membrane surface. Flip-flop of the lipid is a main pathway to release the induced membrane tension. Transient pores with a few water molecules are occasionally observed and are primarily relevant to the flip-flops of the lipid, as illustrated by Figure 7.

Secondary Structure. From the simulations, we can see that (a) AMPs with α-helical structure favor associating with the lipid to form stable and permeable pores inside the membrane. Peptide translocation is occasionally observed for some peptides, such as Melittin. (b) β-sheet peptides can also induce stable pore formation. At the same time, peptide translocation occurs more often. (c) Extended AMPs prefer to translocate across the membrane via short-lived permeable pores. We propose that these behaviors are related to the rigidity and size of the AMPs. Peptides with α-helical structures are the most rigid, and their helical length is usually comparable to the thickness of the membrane. As previously mentioned, the peptides may rotate their orientations and insert into the membrane to release the asymmetrical tension induced by the binding of the peptide. For large and rigid peptides, the rotation requires energy. In contrast, the energy cost is less for rotating smaller sized lipid molecules. Therefore, these rigid peptides facilitate association with lipids to insert into the membrane and form pores. Through the pores, lipid molecules move from the upper leaflet to the lower leaflet and vice versa, whereas the rigid peptides prefer to stably remain in the pore. For example,

dx.doi.org/10.1021/jp505497k | J. Phys. Chem. B XXXX, XXX, XXX−XXX

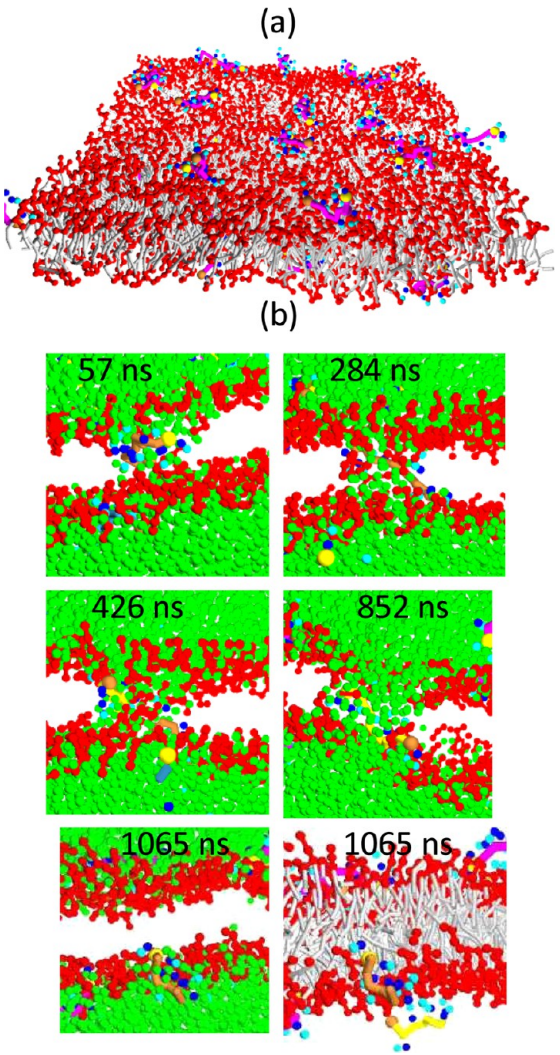

Figure 10. (a) Snapshots of 32 HIV-1 Tat peptides interacting with a bilayer membrane at 1.136 μs. (b) Evolution of a transient pore. To distinguish the peptide, the first peptide that inserts is colored in gold, whereas the second peptide is yellow.

Table 2. Statistics of the Pore Structure and Translocation Induced by Various AMPs[a]

peptide	pore model	number of peptides inside a pore	number of translocated peptide
Magainin 2	disordered toroidal or carpet	2–3 or 5–6	0
MG-H2	disordered toroidal	1–2	3
Melittin	disordered toroidal	2–4	5
CM15	discrete worm-hole	1	1
Protegrin-1	toroidal	2–4	9
Tachyplesin I	disordered toroidal	1–3	7
Indolicidin	irregular barrel-stave	1–3	7
HIV-1 Tat	electroporation	1	14

[a]Data are obtained from simulations at P/L = 2/100 and at a time of 1.136 μS.

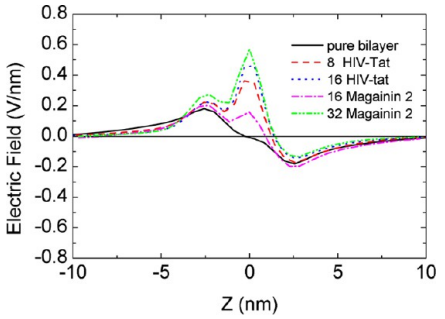

Figure 11. Normal component of the electric field as a function of distance Z from the membrane center for pure DMPC/DMPG bilayer membrane (solid black line), membrane with 8 HIV-1 Tat peptides bound (dashed red line), membrane with 16 HIV-1 Tat peptides bound (dotted blue line), membrane with 16 Magainin peptides bound (dotted-dashed magenta line), and membrane with 32 Magainin peptides bound (dotted-dotted-dashed green line).

through the toroidal pores induced by Magainin 2, MG-H2, and Melittin (see Figures 4–6), lipids exchange (or diffuse) frequently between the two leaflets. Even through the discrete worm-hole pores induced by CM15 (Figures 5d and 7), up to 20 flip-flops of lipids in two directions are observed. We note that Melittin also has the ability to translocate across the membrane. This ability is because Melittin has a kink including three residues in the center of the helix; this kink makes melittin softer than Magainin 2 and MG-H2 and thus makes it easier for melittin to change orientation. Similar to Melittin, β-sheet peptides are relatively more flexible than the α-helical structures, so stable pores and peptide translocations are both observed for Protegrin-1 and Tachyplesin I. In contrast, the extended AMPs, such as Indolicidin, are very flexible and small, and thus it is much easier to change their orientations. These AMPs can insert into and further translocate across the membrane without associating with many lipids.

CONCLUSIONS

In conclusion, our DPD simulations of diverse AMPs interacting with a bilayer membrane give insight into the relationship between the peptide structures and their actions. The cationic charges and amphipathicity are essential for the peptide to bind to the membrane and to disrupt the integrity of the bilayer. In addition, the variety in the secondary structure, the rigidity, and the size of the AMPs is responsible for the complexity and diversity of the pore structure and the translocation pathways. Peptides use these multimodes of action together to maximize the efficiency of their activities. Design of the therapeutic peptide and peptide-mimetics may benefit from our findings. For example, helical or β-sheet formations with well-separated hydrophilic and hydrophobic portions and high rigidity are a good choice to lyse bacterial membrane. Alternatively, extended small peptides bearing sufficient cationic charges should be designed to target cytoplasmic components. Extended peptides can also work as carriers to deliver drugs into a cell.

ASSOCIATED CONTENT

Supporting Information

Movies of Magainin 2 and HIV-1 Tat peptides interacting with bilayer membrane. This material is available free of charge via the Internet at http://pubs.acs.org.

dx.doi.org/10.1021/jp505497k | J. Phys. Chem. B XXXX, XXX, XXX–XXX

AUTHOR INFORMATION

Corresponding Author

*E-mail: lhgao@bnu.edu.cn.

Notes

The authors declare no competing financial interest.

ACKNOWLEDGMENTS

This work is supported by National Science Foundation of China (grant nos. 91127016, 21373031) and the Major State Basic Research Development Programs (grant no. 2011CB808503).

REFERENCES

(1) Zasloff, M. Antimicrobial Peptides of Multicellular Organisms. *Nature* **2002**, *415*, 389−395.

(2) Brogden, K. A. Antimicrobial Peptides: Pore Formers or Metabolic Inhibitors in Bacteria? *Nat. Rev. Microbiol.* **2005**, *3*, 238−250.

(3) Melo, M. N.; Ferre, R.; Castanho, M. A. Antimicrobial Peptides: Linking Partition, Activity and High Membrane-Bound Concentrations. *Nat. Rev. Microbiol.* **2009**, *7*, 245−250.

(4) Fjell, C. D.; Hiss, J. A.; Hancock, R. E.; Schneider, G. Designing Antimicrobial Peptides: Form Follows Function. *Nat. Rev. Drug Discovery* **2012**, *11*, 37−51.

(5) Nguyen, L. T.; Haney, E. F.; Vogel, H. J. The Expanding Scope of Antimicrobial Peptide Structures and Their Modes of Action. *Trends Biotechnol.* **2011**, *29*, 464−472.

(6) Powers, J. P.; Hancock, R. E. The Relationship between Peptide Structure and Antibacterial Activity. *Peptides* **2003**, *24*, 1681−1691.

(7) Matsuzaki, K. Why and How Are Peptide Lipid Interactions Utilized for Self-Defense? Magainins and Tachyplesins as Archetypes. *Biochim. Biophys. Acta* **1999**, *1462*, 1−10.

(8) Shai, Y. Mechanism of the Binding, Insertion and Destabilization of Phospholipid Bilayer Membranes by α-helical Antimicrobial and Cell Non-Selective Membrane-Iytic Peptides. *Biochim. Biophys. Acta, Biomembr.* **1999**, *1462*, 55−70.

(9) Yang, L.; Weiss, T. M.; Lehrer, R. I.; Huang, H. W. Crystallization of Antimicrobial Pores in Membranes: Magainin and Protegrin. *Biophys. J.* **2000**, *79*, 2002−2009.

(10) Leontiadou, H.; Mark, A. E.; Marrink, S. J. Antimicrobial Peptides in Action. *J. Am. Chem. Soc.* **2006**, *128*, 12156−12161.

(11) Lin, J.-H.; Baumgaertner, A. Stability of a Melittin Pore in a Lipid Bilayer: a Molecular Dynamics Study. *Biophys. J.* **2000**, *78*, 1714−1724.

(12) Herce, H. D.; Garcia, A. E. Molecular Dynamics Simulations Suggest a Mechanism for Translocation of the HIV-1 TAT Peptide across Lipid Membranes. *Proc. Natl. Acad. Sci. U.S.A.* **2007**, *104*, 20805−20810.

(13) Cirac, A. D.; Moiset, G.; Mika, J. T.; Kocer, A.; Salvador, P.; Poolman, B.; Marrink, S. J.; Sengupta, D. The Molecular Basis for Antimicrobial Activity of Pore-Forming Cyclic Peptides. *Biophys. J.* **2011**, *100*, 2422−2431.

(14) Smit, B.; Hilbers, P.; Esselink, K.; Rupert, L.; Van Os, N.; Schlijper, A. Computer Simulations of a Water/Oil Interface in the Presence of Micelles. *Nature* **1990**, *348*, 624−625.

(15) Klein, M. L.; Shinoda, W. Large-Scale Molecular Dynamics Simulations of Self-Assembling Systems. *Science* **2008**, *321*, 798−800.

(16) Illya, G.; Deserno, M. Coarse-Grained Simulation Studies of Peptide-Induced Pore Formation. *Biophys. J.* **2008**, *95*, 4163−4173.

(17) Monticelli, L.; Kandasamy, S. K.; Periole, X.; Larson, R. G.; Tieleman, D. P.; Marrink, S.-J. The MARTINI Coarse-Grained Force Field: Extension to Proteins. *J. Chem. Theory Comput.* **2008**, *4*, 819−834.

(18) Gao, L.; Fang, W. Effects of Induced Tension and Electrostatic Interactions on the Mechanisms of Antimicrobial Peptide Translocation across Lipid Bilayer. *Soft Matter* **2009**, *5*, 3312−3318.

(19) Chen, L.; Gao, L. How the Antimicrobial Peptides Kill Bacteria: Computational Physics Insights. *Commun. Comput. Phys.* **2012**, *11*, 709−725.

(20) Chen, L.; Jia, N.; Gao, L.; Fang, W.; Golubovic, L. Effects of Antimicrobial Peptide Revealed by Simulations: Translocation, Pore formation, Membrane Corrugation and Euler Buckling. *Int. J. Mol. Sci.* **2013**, *14*, 7932−7958.

(21) Espanol, P.; Warren, P. Statistical Mechanics of Dissipative Particle Dynamics. *Eur. Phys. Lett.* **1995**, *30*, 191−196.

(22) Groot, R. D.; Warren, P. B. Dissipative Particle Dynamics: Bridging the Gap between Atomistic and Mesoscopic Simulation. *J. Chem. Phys.* **1997**, *107*, 4423−4435.

(23) Shillcock, J. C.; Lipowsky, R. Equilibrium Structure and Lateral Stress Distribution of Amphiphilic Bilayers from Dissipative Particle Dynamics Simulations. *J. Chem. Phys.* **2002**, *117*, 5048−5061.

(24) Gao, L.; Shillcock, J.; Lipowsky, R. Improved Dissipative Particle Dynamics Simulations of Lipid Bilayers. *J. Chem. Phys.* **2007**, *126*, 015101.

(25) Marrink, S. J.; de Vries, A. H.; Mark, A. E. Coarse Grained Model for Semiquantitative Lipid Simulations. *J. Phys. Chem. B* **2004**, *108*, 750−760.

(26) Marrink, S. J.; Risselada, H. J.; Yefimov, S.; Tieleman, D. P.; de Vries, A. H. The MARTINI Force Field: Coarse Grained Model for Biomolecular Simulations. *J. Phys. Chem. B* **2007**, *111*, 7812−7824.

(27) Groot, R.; Rabone, K. Mesoscopic Simulation of Cell Membrane Damage, Morphology Change and Rupture by Nonionic Surfactants. *Biophys. J.* **2001**, *81*, 725−736.

(28) Vishnyakov, A.; Talaga, D. S.; Neimark, A. V. DPD Simulation of Protein Conformations: From α-helices to β-Structures. *J. Phys. Chem. Lett.* **2012**, *3*, 3081−3087.

(29) Groot, R. D. Electrostatic Interactions in Dissipative Particle Dynamics-Simulation of Polyelectrolytes and Anionic Surfactants. *J. Chem. Phys.* **2003**, *118*, 11265.

(30) Gao, L.; Fang, W. Communications: Self-Energy and Corresponding Virial Contribution of Electrostatic Interactions in Dissipative Particle Dynamics: Simulations of Cationic Lipid Bilayers. *J. Chem. Phys.* **2010**, *132*, 031102.

(31) Jakobsen, A. F. Constant-Pressure and Constant-Surface Tension Simulations in Dissipative Particle Dynamics. *J. Chem. Phys.* **2005**, *122*, 124901.

(32) Ludtke, S. J.; He, K.; Heller, W. T.; Harroun, T. A.; Yang, L.; Huang, H. W. Membrane Pores Induced by Magainin. *Biochemistry* **1996**, *35*, 13723−13728.

(33) Lee, M. T.; Sun, T. L.; Hung, W. C.; Huang, H. W. Process of Inducing Pores in Membranes by Melittin. *Proc. Natl. Acad. Sci. U.S.A.* **2013**, *110*, 14243−14248.

(34) Pistolesi, S.; Pogni, R.; Feix, J. B. Membrane Insertion and Bilayer Perturbation by Antimicrobial Peptide CM15. *Biophys. J.* **2007**, *93*, 1651−1660.

(35) Bechinger, B. Structure and Functions of Channel-Forming Peptides: Magainins, Cecropins, Melittin and Alamethicin. *J. Membr. Biol.* **1997**, *156*, 197−211.

(36) Mihajlovic, M.; Lazaridis, T. Charge Distribution and Imperfect Amphipathicity Affect Pore Formation by Antimicrobial Peptides. *Biochim. Biophys. Acta* **2012**, *1818*, 1274−1283.

(37) Gidalevitz, D.; Ishitsuka, Y.; Muresan, A. S.; Konovalov, O.; Waring, A. J.; Lehrer, R. I.; Lee, K. Y. Interaction of Antimicrobial Peptide Protegrin with Biomembranes. *Proc. Natl. Acad. Sci. U.S.A.* **2003**, *100*, 6302−6307.

(38) Bolintineanu, D.; Hazrati, E.; Davis, H. T.; Lehrer, R. I.; Kaznessis, Y. N. Antimicrobial Mechanism of Pore-Forming Protegrin Peptides: 100 Pores to Kill E. Coli. *Peptides* **2010**, *31*, 1−8.

(39) Matsuzaki, K.; Yoneyama, S.; Fujii, N.; Miyajima, K.; Yamada, K.-i.; Kirino, Y.; Anzai, K. Membrane Permeabilization Mechanisms of a Cyclic Antimicrobial Peptide, Tachyplesin I, and its Linear Analog. *Biochemistry* **1997**, *36*, 9799−9806.

(40) Subbalakshmi, C.; Sitaram, N. Mechanism of Antimicrobial Action of Indolicidin. *FEMS Microbiol. Lett.* **1998**, *160*, 91−96.

(41) Falla, T. J.; Karunaratne, D. N.; Hancock, R. E. Mode of Action of the Antimicrobial Peptide Indolicidin. *J. Biol. Chem.* **1996**, *271*, 19298−19303.
(42) Vives, E.; Brodin, P.; Lebleu, B. A. Truncated HIV-1 Tat Protein Basic Domain Rapidly Translocates Through the Plasma Membrane and Accumulates in the Cell Nucleus. *J. Biol. Chem.* **1997**, *272*, 16010−16017.
(43) Jean-Francois, F.; Elezgaray, J.; Berson, P.; Vacher, P.; Dufourc, E. J. Pore Formation Induced by an Antimicrobial Peptide: Electrostatic Effects. *Biophys. J.* **2008**, *95*, 5748−5756.
(44) Tieleman, D.; Leontiadou, H.; Mark, A.; Marrink, S. Simulation of Pore Formation in Lipid Bilayers by Mechanical Stress and Electric Fields. *J. Am. Chem. Soc.* **2003**, *125*, 6382−6383.
(45) Gurtovenko, A. A.; Vattulainen, I. Pore Formation Coupled to Ion Transport through Lipid Membranes as Induced by Transmembrane Ionic Charge Imbalance: Atomistic Molecular Dynamics Study. *J. Am. Chem. Soc.* **2005**, *127*, 17570−17571.
(46) Fantner, G. E.; Barbero, R. J.; Gray, D. S.; Belcher, A. M. Kinetics of Antimicrobial Peptide Activity Measured on Individual Bacterial Cells Using High-Speed Atomic Force Microscopy. *Nat. Nanotechnol.* **2010**, *5*, 280−285.